The reactivity of ethylene oxide in contact with iron oxide fines as measured by adiabatic calorimetry

M.E. Levin[*]

Shell Global Solutions (US) Inc., P.O. Box 1380, Houston, TX 77251-1380, USA

Abstract

Samples of various iron oxides suspended above ethylene oxide in an adiabatic calorimeter exhibit exothermic activity at temperatures as low as room temperature. A γ-Fe_2O_3 sample was found to show the highest reactivity with ethylene oxide. Ethylene oxide in combination with most of the iron oxide fines tested displayed exothermic activity below 100 °C. Self-heat rates near 2000 °C/min were observed for the γ-Fe_2O_3 fines while rates in excess of 100 °C/min were found for other fines (α-Fe_2O_3 and hydrated α-Fe_2O_3). In two cases (α-Fe_3O_4 and α-Fe_2O_3), pressurization rates above 1000 psi/min took place. No reactivity was observed for ethylene oxide with the FeO. Thermal inertia effects in commercial operation, such as heat uptake by the equipment to which fines are attached, are presumed to be a factor in limiting the occurrence of related exotherms in ethylene oxide manufacturing facilities.
© 2003 Shell International Chemicals B.V. Published by Elsevier B.V.

Keywords: Ethylene oxide; Iron oxide; γ-Fe_2O_3; α-Fe_2O_3; α-Fe_3O_4; FeO; Reactivity; Calorimetry; APTAC[TM]

1. Introduction

1.1. Background

Ethylene oxide is known to undergo a variety of reactions, such as isomerization, polymerization, disproportionation, and decomposition, under appropriate conditions [1,2]. It can also react when in contact with numerous other species. Reaction of ethylene oxide with water and ethylene glycol over a wide range of concentrations has recently been extensively studied [3]. The occurrence of such reactions under uncontrolled circumstances can pose a significant threat to personnel and can cause equipment damage.

An explosion at the Union Carbide Seadrift ethylene oxide plant claimed the life of one worker and caused extensive equipment damage in 1991. Union Carbide conducted an extensive investigation in the aftermath of this incident to understand what had transpired,

---
* Tel.: +1-281-544-7575; fax: +1-281-544-7705.
E-mail address: marc.levin@shell.com (M.E. Levin).

what factors contributed to the event, what (if any) new findings were uncovered, and what measures might be applied to prevent similar incidents. Much of the information developed in the investigation was shared with other ethylene oxide manufacturers and with ethylene oxide customers [4–7]. As part of the incident investigation, numerous studies of the reactivity and ignition characteristics of ethylene oxide with various forms of iron oxide were conducted. One of the key findings in the investigation was the role a seldom-encountered form of iron oxide, γ-Fe_2O_3, played in the sequence of events. In addition, the insulating and reservoir-like characteristics of ethylene oxide polymer were identified as important contributors.

In response to what was made known about the Union Carbide experience, Shell Chemicals[1] conducted a review of their own manufacturing facilities to see what configurations and conditions might be similar. As one outgrowth from that review, the reactivity of ethylene oxide with various forms of iron oxide was examined to determine if this chemistry could take place in any of our plants. The current study presents findings from adiabatic calorimetry employed to characterize the reactivity of ethylene oxide with iron oxide fines.

2. Experimental

2.1. Equipment

Testing for this study was carried out in the Automatic Pressure Tracking Adiabatic Calorimeter (APTAC^{TM}) now available from TIAX, LLC. The instrument operates on the principle of minimizing the heat loss from the sample and sample cell by heating the gas space surrounding the cell to match the sample temperature. This allows a sample undergoing an exothermic reaction to self-heat at a rate and extent comparable to that in a large-scale, adiabatic environment. The sample cell resides in a containment vessel equipped with heaters and thermocouples for this purpose. A thermocouple is also placed inside the sample cell. The internals of the APTAC^{TM} are depicted in Fig. 1.

The instrument also adjusts the pressure in the containment vessel to match the pressure in the cell allowing for a relatively thin-wall sample container. Sample pressures reaching nearly 2000 psia (13,800 kPa) can be accommodated. A thin-wall 2.5 in. titanium sample cell is employed to limit the amount of heat absorbed from the sample. The relative thermal capacitance of the cell plus sample to the sample alone is expressed by the thermal inertia factor, ϕ:

$$\phi = 1 + \frac{m_c C_{p_c}}{m_s C_{p_s}}$$

where m denotes the mass, C_p the heat capacity, subscript c the cell + stir bar, and s the sample. The ϕ factor of industrial equipment approaches a value of unity; a value of 1.15–1.30 is typical of APTAC^{TM} tests.

Stirring is accomplished via a Teflon-coated magnetic stir bar inserted in the sample cell. Three-zone heating is provided in the containment vessel along with an additional heater for

---

[1] The expression "Shell Chemicals" refers to the companies of the Royal Dutch/Shell Group, which are engaged in chemical businesses. Each of the companies which make up the Royal Dutch/Shell Group of companies is an independent entity and has its own separate identity.
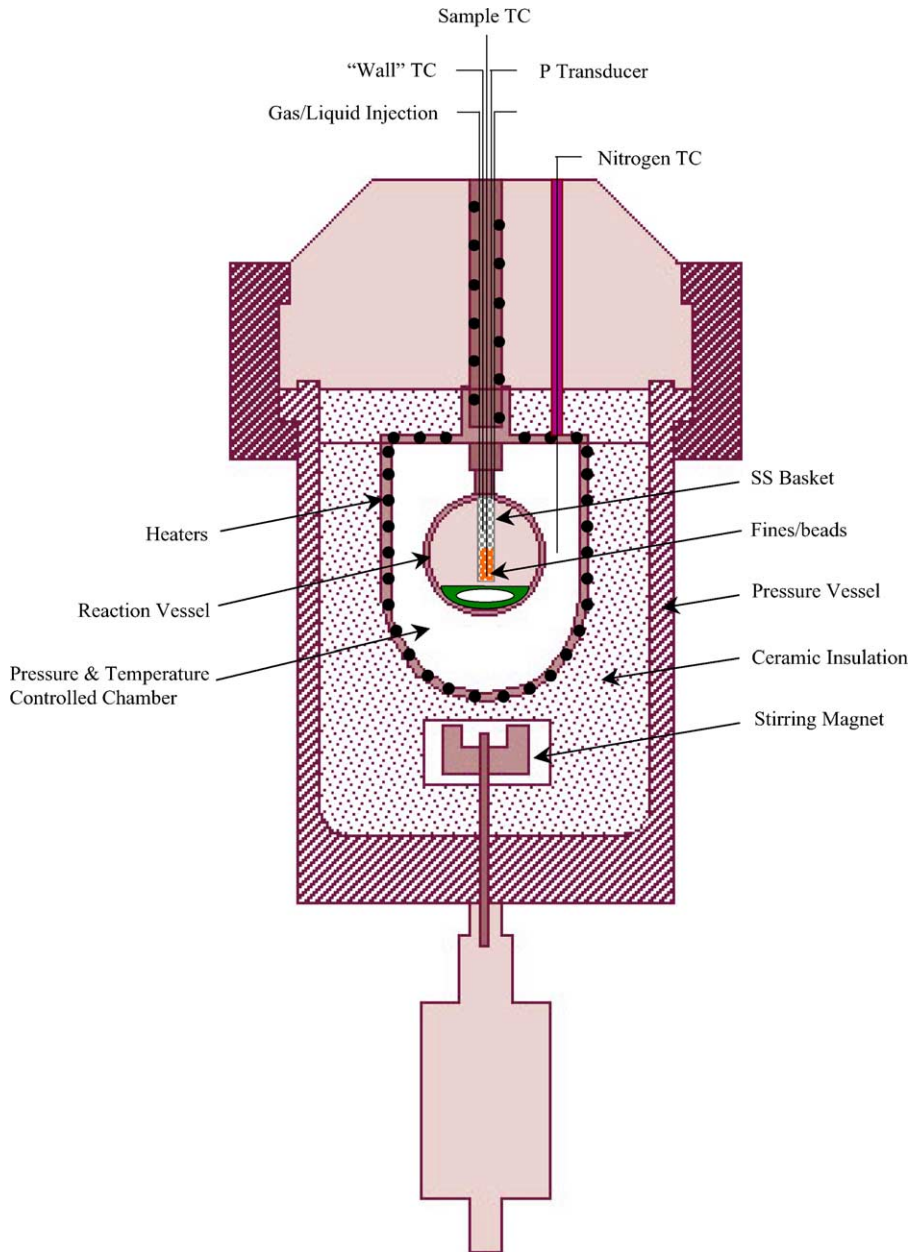
Fig. 1. Depiction of the Automatic Pressure Tracking Adiabatic Calorimeter (APTAC^TM).

the tubing bundle connected to the sample cell. The APTAC[TM] can match temperature and pressure rise rates of up to 400 °C/min and 10,000 psi/min (69,000 kPa/min), respectively.

APTAC[TM] operation is typically in the heat-wait-search (H-W-S) mode. That is, the sample is heated to a pre-selected temperature and upon reaching this temperature, the instrument waits for a period of time (usually 25 min) for the cell and containment vessel temperatures to stabilize. After the wait period, the instrument continues at that temperature (for another 25 min) to determine if there is any exothermic activity. During this time, the temperature of the containment vessel gas space is adjusted to match that of the sample thermocouple. If no heat-up activity exceeding a pre-set self-heating rate threshold is observed, it is concluded that there is no exotherm. The sample is then heated to the next temperature and the process repeated. If an exotherm is detected, the APTAC[TM] tracks the sample conditions and adjusts the temperature and pressure of the containment vessel accordingly (adiabatic or exotherm mode).

APTAC[TM] exotherm thresholds of 0.05 °C/min (versus the quoted 0.04 °C/min detection limit) were employed to reduce the likelihood of the occurrence of "drift" (in which a slight thermocouple calibration imbalance yields a slow temperature rise rate and is interpreted as an exotherm).

For the purpose of this study, iron oxide fines and glass beads were suspended in a stainless-steel basket within the APTAC[TM] sample cell. Baskets are made of 200 mesh SS screen spot-welded to form a cylinder. Another piece of screen was spot-welded to form the bottom; the top was spot-welded to a 3/8 in. stainless steel Swagelok® back ferrule to retain the shape of the basket and to prevent slippage of the basket into the APTAC[TM] sample cell. The baskets are 2.5 in. in height and 0.42 in. in diameter. A basket weight is typically 0.92 g. Fines or beads were charged to the basket and the sample thermocouple was embedded within the section occupied by fines in the basket. The "wall" thermocouple, which is normally placed against the *outside* of the sample cell, was routed through one of the four remaining 1/16 in. sample cell access lines and into the gas-phase portion of the basket.

Given the basket configuration in this study and the likelihood that any observed reaction is taking place on the iron oxide fines, the normal definition of the thermal inertia factor, ϕ, described above is not meaningful for this system. In actuality, ϕ for these tests is likely much greater than unity since the mass of the iron oxide fines is much larger than the mass of vapor-phase ethylene oxide in immediate contact with the fines. For this reason, values for the thermal inertia factors for the tests in this study are not reported.

2.2. Samples

Ethylene oxide lecture bottles, purchased from Aldrich (#38,761-4), were employed in this study.

A variety of solids were tested to determine reactivity with ethylene oxide, including

γ-Fe_2O_3	Aldrich #48,066-5
α-Fe_2O_3	Aldrich #20,351-3
α-Fe_2O_3, hydrated	Aldrich #37,125-4
Fe_3O_4	Alfa Aesar #12962
FeO	Alfa Aesar #30513
Glass beads	Baxter #G6000-1

2.3. Procedures

As is normally the case prior to liquid-phase studies, the APTAC[TM] was calibrated beforehand by mounting an empty cell in the calorimeter and determining temperature offsets at 50 °C intervals between 50 and 400 °C beginning at a total nitrogen pressure of 500 psia (3450 kPa). This procedure is expected to be appropriate for the study of gas–solid reactions in the calorimeter. The calibration procedure is an automated feature of the APTAC[TM].

To preclude reaction with oxygen, steps were taken in all experiments to minimize exposure to air. Liquid ethylene oxide was collected by attaching the lecture bottle (a compressed gas sample cylinder) to a dry ice/acetone-cooled condenser. Once sufficient material was collected in the condenser's graduated trap, the material was transferred by cannula under nitrogen pressure into a dry ice/acetone-cooled APTAC[TM] sample cell (fitted with a septum and purged with nitrogen). The sample cell was then placed in a glove bag.

Roughly 0.5 g of fines (or glass beads) were charged into a SS basket and also placed into the glove bag. After attaching the glove bag to the APTAC[TM] containment vessel head and purging with five vacuum/nitrogen cycles, the sample cell septum was removed. The basket was then fitted around the sample and wall thermocouples, inserted into the sample cell, and the sample cell was then attached to the vessel head.

Total EO sample weights ranged from 19.1 to 20.5 g and solids weights ranged from 0.47 to 0.50 g, while the total weight of titanium cell and stir bar ranged between 34.3 and 38.7 g.

No gas samples for compositional analysis were taken at the end of any of the tests. A summary of test characteristics may be found in Table 1.

3. Results and discussion

3.1. Ethylene oxide + empty basket, glass, or α-FeO

The combinations of ethylene oxide with either an empty basket, a basket containing glass beads, or a basket with α-FeO fines were examined first. Fig. 2 depicts the temperature versus time behavior for these three cases. The appearance of self-heating of ethylene oxide with an empty basket starts at about 60 °C and continued to 165 °C with the experiment effectively ending thereafter. In contrast, when the basket contains either glass beads or α-FeO fines, only the typical stair-step behavior of the heat-wait-search (H-W-S) mode is seen. In the case of the α-FeO, heat-wait-search steps to above 250 °C were carried out. The stair-step behavior suggests the absence of any discernable exothermic activity of ethylene oxide in this environment. Parallel trends are exhibited in the pressure versus time plot of Fig. 3. Ethylene oxide with the empty basket shows some increase in pressure with time while the glass- and α-FeO-containing baskets only display the H-W-S behavior.

Fig. 4 shows differences in temperature between the material in the basket and the ethylene oxide in the gas phase during the tests. In the α-FeO test, the solids thermocouple is as much as 15 °C higher in temperature than the gas-phase thermocouple. However, as will be seen later, this is actually a relatively-small difference in temperature. For the empty basket and the glass bead-containing basket, the solids were as much as 7 °C higher temperature than the gas phase and at other times during the test, were even 9 °C below the gas phase temperature.

Table 1
Summary of APTAC[TM] test conditions and results for ethylene oxide plus iron oxide fines

Run ID	A00364	A00371	A00506	A00509	A00507	A00510
Date	16 November 2000	18 December 2000	27 November 2001	4 December 2001	29 November 2001	6 December 2001
LR	LR24922-65	LR24922-76	LR25132-113	LR25132-117	LR25132-114	LR25132-118
Fines	None	Glass beads	FeO	FeO	Fe_3O_4	Fe_3O_4
Source	–	Baxter #G6000-1	Alfa Aesar #30513	Alfa Aesar #30513	Alfa Aesar #12962	Alfa Aesar #12962
EO mass (g)	20.14	20.17	19.72	19.68	20.18	20.16
Fines mass (g)	–	0.49	0.50	0.52	0.51	0.50
Sample cell mass (titanium) (g)	30.55	30.83	32.20	32.19	31.85	31.71
Stir bar mass (g)	3.45	3.35	3.42	3.38	3.42	3.35
Stirring rate (magnetic) (rpm)	500	500	500	500	500	500
Expt. (search) start temperature (°C)	60	25	25	35	25	27
Expt. final or maximum temperature (°C)	340	340	340	340	340	340
Heat-wait-search increment (°C)	10	10	10	10	10	10
Expt. Exotherm limit (N_2) (°C)	360	360	360	360	360	360
Expt. Temperature shutdown (°C)	360	350	360	360	360	360
Expt. pressure shutdown (psia)	1800	1800	1800	1800	1800	1800
Expt. heat rate shutdown (°C/min)	400	350	400	400	400	400
Expt. press rate shutdown (psi/min)	10000	5000	10000	10000	10000	10000
Exotherm threshold (°C/min)	0.05	0.05	0.05	0.05	0.05	0.05
Number of exotherms	1	0	–	–	4 + ?	4 + ?
Observed onset temperature (0.06 °C/min) (°C)	61	–	–	–	12	?
Maximum observed temperature (within exotherm) (°C)	165	255	–	–	899[c]	390
Maximum observed pressure (psia)	707	1110	–	–	1798	1330
Maximum observed self-heat rate[a] (°C/min)	38	–	–	–	41700[b]	38
Maximum observed pressure rate[a] (psi/min)	17	–	–	–	118	39
Temperature at maximum self-heat rate[a] (°C)	127	–	–	–	899	351
Temperature at maximum pressure rate[a] (°C)	164	–	–	–	826	380
Expt. duration (before S/D) (min)			1560	1152	862	910
Expt. shutdown cause	Uncertain	Manual	Manual	Manual	Exotherm limit	Exotherm limit
Comments	Unclear how much may be drift vs. actual exotherm				Possible poor solids TC contact—T jumping after 900 °C; cell & RD rupture	

Table 1 (*Continued*)

Run ID	A00370	A00367	A00362	A00363	A00373
Date	12 December 2000	28 November 2000	15 November 2000	16 November 2000	18 December 2000
LR	LR24922-75	LR24922-70	LR24922-63	LR24922-64	LR24922-79
Fines	α-Fe$_2$O$_3$	Hydrated α-Fe$_2$O$_3$	γ-Fe$_2$O$_3$	γ-Fe$_2$O$_3$	γ-Fe$_2$O$_3$
Source	Aldrich #20,351-3	Aldrich #37,125-4	Aldrich #48,066-5	Aldrich #48,066-5	Aldrich #48,066-5
EO mass (g)	20.29	19.98	20.49	19.90	19.95
Fines mass (g)	0.50	0.50	0.49	0.47	0.50
Sample cell mass (titanium) (g)	31.58	31.45	30.98	32.15	32.53
Stir bar mass (g)	3.44	3.37	3.38	3.40	3.35
Stirring rate (magnetic) (rpm)	500	500	500	500	500
Expt. (search) start temperature (°C)	25	25	60	25	25
Expt. final or maximum temperature (°C)	340	340	340	340	340
Heat-wait-search increment (°C)	10	10	10	10	10
Expt. exotherm limit (N$_2$) (°C)	360	360	360	360	360
Expt. temperature shutdown (°C)	350	360	360	360	360
Expt. pressure shutdown (psia)	1800	1800	1800	1800	1800
Expt. heat rate shutdown (°C/min)	350	400	400	400	400
Expt. press rate shutdown (psi/min)	5000	10000	10000	10000	10000
Exotherm threshold (°C/min)	0.05	0.05	0.05	0.05	0.05
Number of exotherms	1+	1+	1	1+	1
Observed onset temperature (0.06 °C/min) (°C)	52	34	(10)	(4)	(12)
Maximum observed temperature (within exotherm) (°C)	763	358	599	469	620
Maximum observed pressure (psia)	2680	1150	97	64	173
Maximum observed self-heat rate[a] (°C/min)	16800[b]	203	1790[b]	1600[b]	1180
Maximum observed pressure rate[a] (psi/min)	1420	255	21	6.2	47
Temperature at maximum self-heat rate[a] (°C)	643	272	197	315	189
Temperature at maximum pressure rate[a] (°C)	526	277	542	105*	522
Expt. duration (before S/D) (min)	1285	704	13.6	14.3	16.9
Expt. shutdown cause	Exotherm limit; cell & RD rupture	Blown fuse	Heat rate S/D	Heat rate S/D	Htr Power
Comments					

EO from Aldrich #38,761-4; nitrogen pad gas; parentheses ( ) denote extrapolation to lower temperature.

[a] During exotherm.

[b] Self-heat rate sufficiently high to cause possible temperature reading lag.
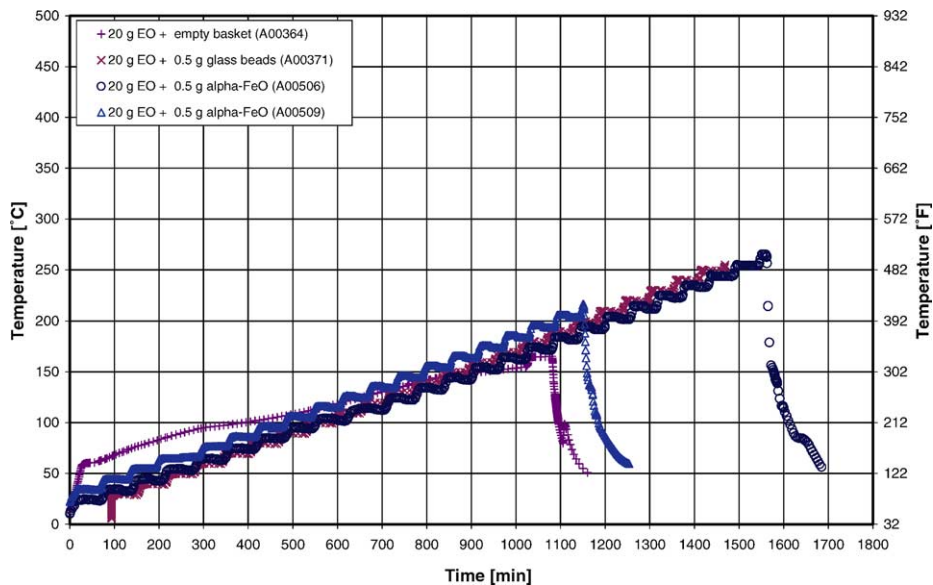
[c] Reached equipment maximum reading.

Fig. 2. Temperature history of ethylene oxide in contact with glass and α-FeO in the APTAC[TM].

The self-heat rate behavior of these three systems is displayed in the self-heat rate versus reciprocal temperature plot of Fig. 5. The empty basket shows only marginal self-heating (that is, less than 0.2 °C/min for the most part) and only the portion above 97 °C exhibits a behavior characteristic of Arrhenius-type kinetics. It is not clear whether the observed behavior
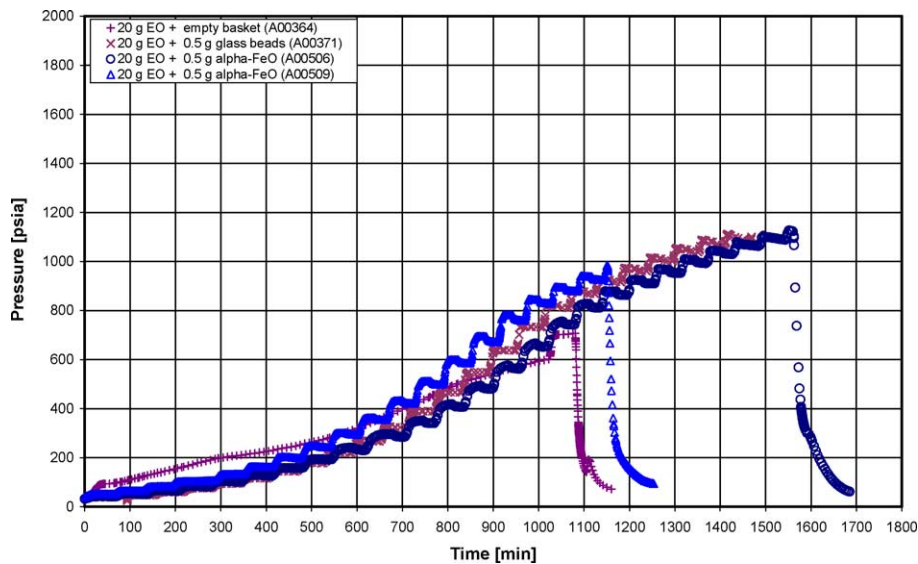

Fig. 3. Pressure history of ethylene oxide in contact with glass and α-FeO in the APTAC[TM].
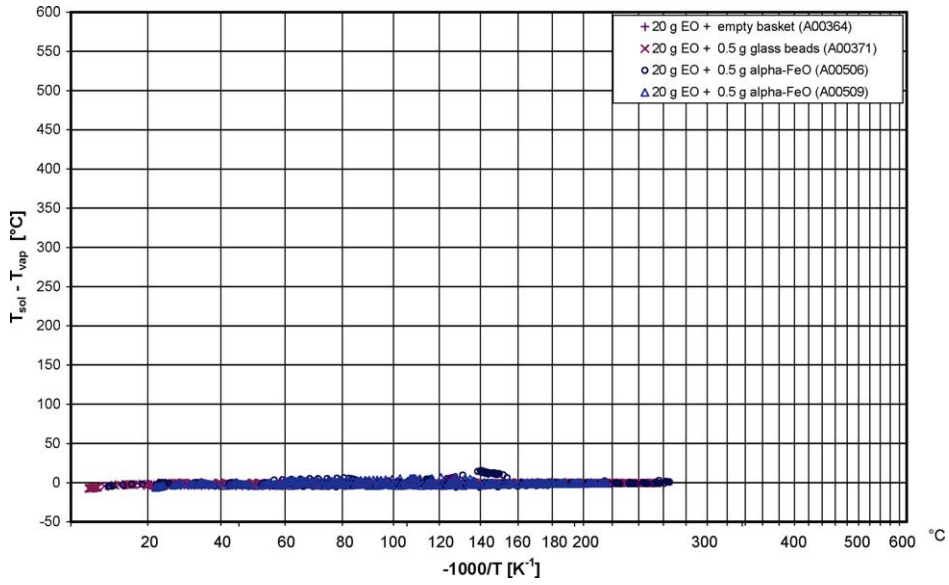
Fig. 4. Temperature difference between solid and gas phase of ethylene oxide in contact with glass and α-FeO in the APTAC^{TM}.
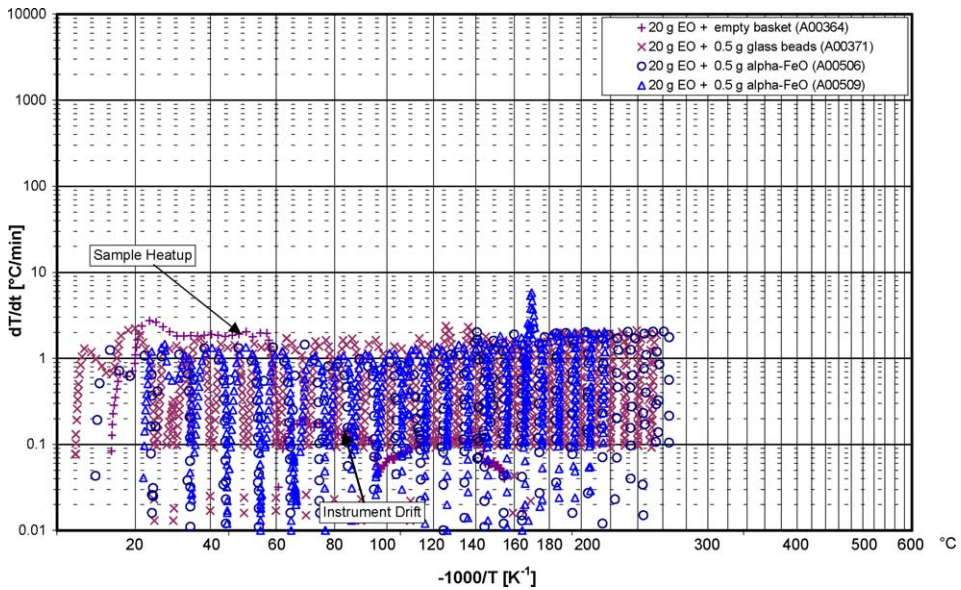
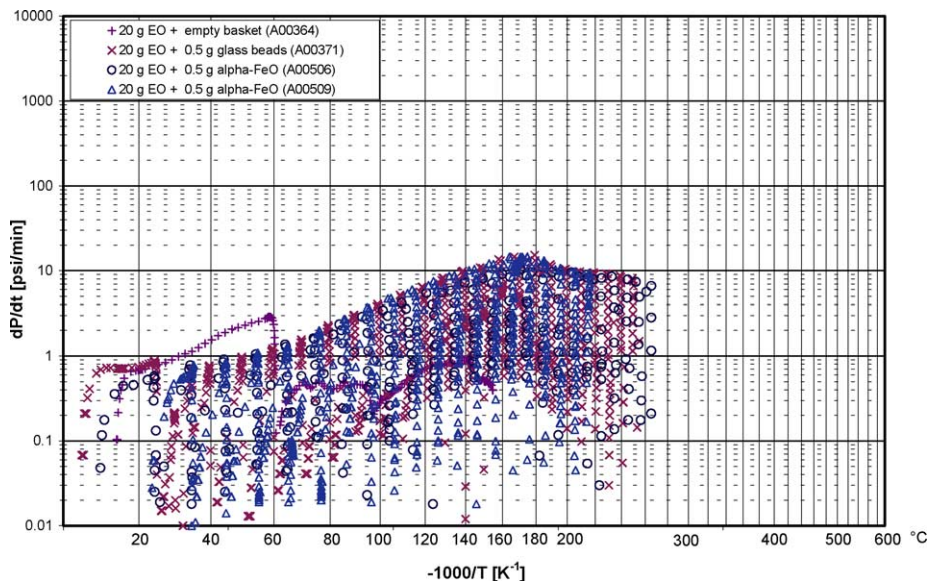Fig. 5. Self-heat rate profiles of ethylene oxide in contact with glass and α-FeO in the APTAC^{TM}.

Fig. 6. Pressurization rate profiles of ethylene oxide in contact with glass and α-FeO in the APTAC$^{\text{TM}}$.

for the empty basket is actually an exotherm or just experimental drift. The stair-step behavior of the glass beads and α-FeO appears in this plot as the repeated heat-up peaks followed by diminished dT/dt values (as the instrument attempted at each step to allow the temperature to stabilize and then to look for an exotherm). No exotherms are apparent for these particular solids.

The corresponding pressurization profiles as a function of reciprocal temperature are shown in Fig. 6. Besides the absence of any features that might be associated with a significant exotherm, there is no evidence of generation of non-condensible gas or light vapor species. The pressure–temperature plot of Fig. 7 reflects this, as well, in that the cool-down pressure at a given temperature in each test does not lie above the heat-up pressure. In the case of ethylene oxide with α-FeO, the cool-down pressure seems to lie *below* the heat-up pressure suggesting that some conversion of ethylene oxide to a less volatile species may be taking place. If this is occurring, the reaction energetics and/or rate must be sufficiently low to avoid self-heat rate detection by the instrument.

3.2. Ethylene oxide + iron oxide fines (α-Fe$_3$O$_4$, α-Fe$_2$O$_3$, hydrated α-Fe$_2$O$_3$, and γ-Fe$_2$O$_3$)

The temperature versus time behavior of a variety of commercially-available iron oxides suspended in the stainless steel basket above the ethylene oxide is displayed in Fig. 8. In contrast to the trends exhibited by glass beads or the α-FeO, exothermic behavior is clearly evident. For each of the iron oxides in this group (α-Fe$_3$O$_4$, α-Fe$_2$O$_3$, hydrated α-Fe$_2$O$_3$, γ-Fe$_2$O$_3$), a sharp, upward spike in temperature takes place. For the γ-Fe$_2$O$_3$ sample, reaction appears to occur near room temperature. With the exception of the hydrated α-Fe$_2$O$_3$
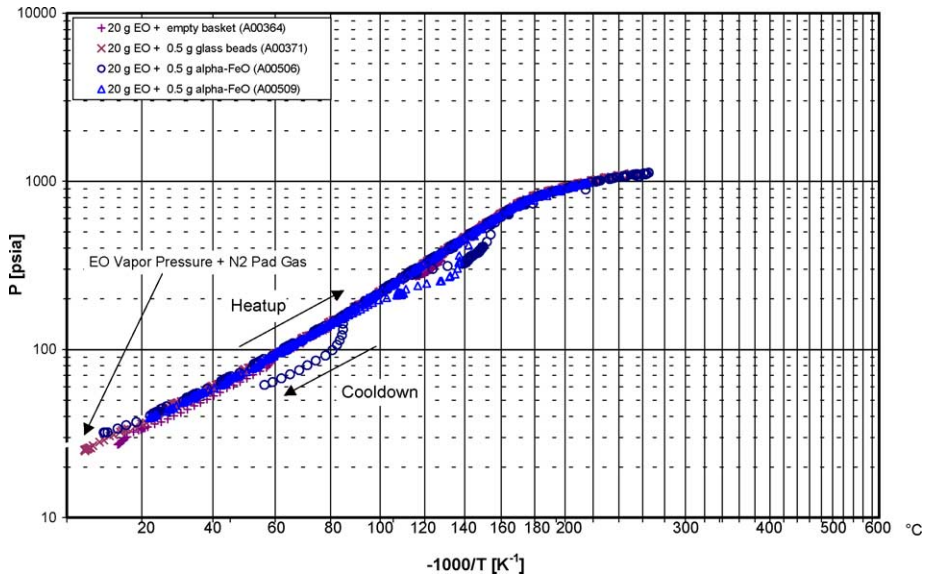
Fig. 7. Pressure–temperature profiles of ethylene oxide in contact with glass and α-FeO in the APTAC[TM].
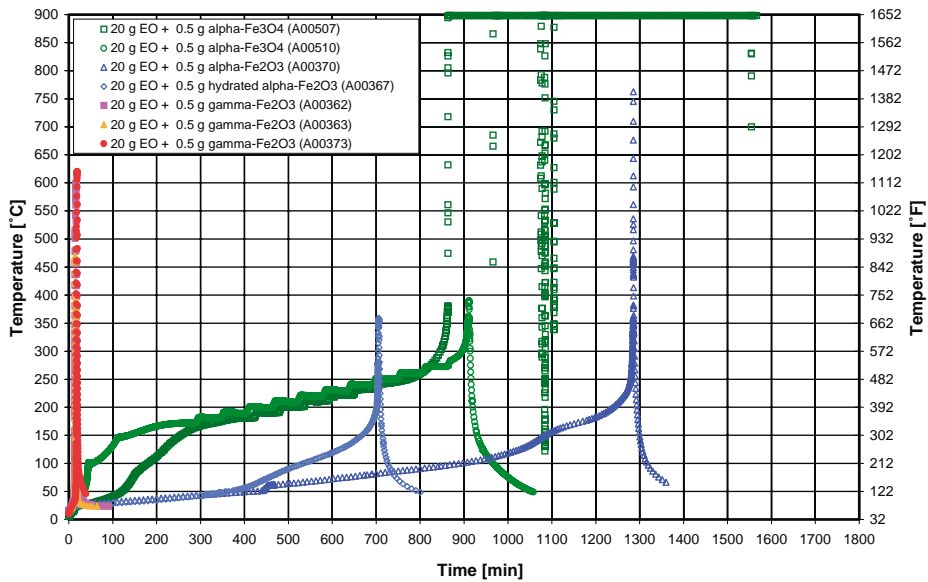

Fig. 8. Temperature history of ethylene oxide in contact with iron oxide in the APTAC[TM].
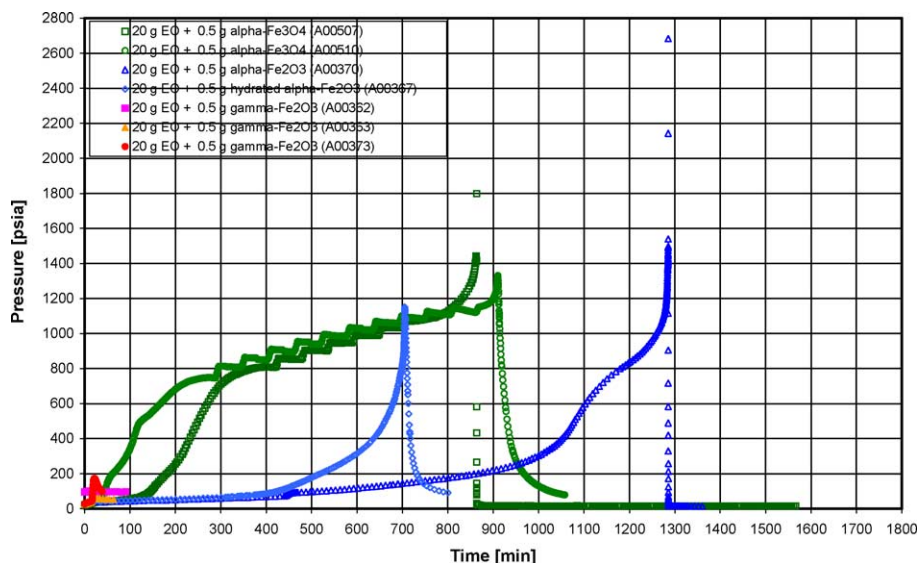
Fig. 9. Pressure history of ethylene oxide in contact with iron oxide in the APTAC[TM].

and one α-Fe$_3$O$_4$ test (which appears to have encountered a programmed instrument shut-down), temperatures ultimately exceed 600 °C. On the other hand, the other α-Fe$_3$O$_4$ test resulted in a temperature pegged the instrument thermocouple at 900 °C. The shapes of the α-Fe$_3$O$_4$ and α-Fe$_2$O$_3$ curves (and possibly the hydrated α-Fe$_2$O$_3$) suggest the occurrence of multiple peaks or reactions taking place.

Pressures in excess of 1000 psia (6900 kPa) were generated for the α-Fe$_3$O$_4$, α-Fe$_2$O$_3$, and hydrated α-Fe$_2$O$_3$ solids (Fig. 9). For the case of α-Fe$_2$O$_3$, the maximum pressure reached was about 2700 psia (18,600 kPa). For the three tests involving γ-Fe$_2$O$_3$, the peak pressure did not exceed 200 psia (1380 kPa). Again, multiple peak behavior is apparent in several of the tests, particularly for α-Fe$_3$O$_4$ and α-Fe$_2$O$_3$.

The temperature difference between the solid and gas phases as a function of tempera-ture, illustrated in Fig. 10, exhibits some relatively complex trends. It is clear that the solids temperature can be substantially greater than the vapor-phase temperature, strongly sug-gesting that reaction is taking place on or in the solids. In two γ-Fe$_2$O$_3$ tests, the solids are 450 °C higher in temperature than the vapor phase and in one α-Fe$_3$O$_4$ test, the solids are more than 600 °C higher in temperature. In addition, there appears to be a hysteresis-like effect, in which the solid–vapor temperature difference depends on whether the system is in a heat-up mode (reaction) or cool-down mode (shutdown).

The rates of reaction of the various iron oxide fines with ethylene oxide are reflected in the self-heat rate plot of Fig. 11. This graph displays temperature rise rate versus negative reciprocal temperature (with the corresponding temperatures in °C shown). The reaction rate can be found by multiplying the self-heat rate by the sample heat capacity and dividing by the heat of reaction. The same self-heat rate versus temperature curves are displayed in Fig. 12 with the heat-wait-search steps removed for clarity.
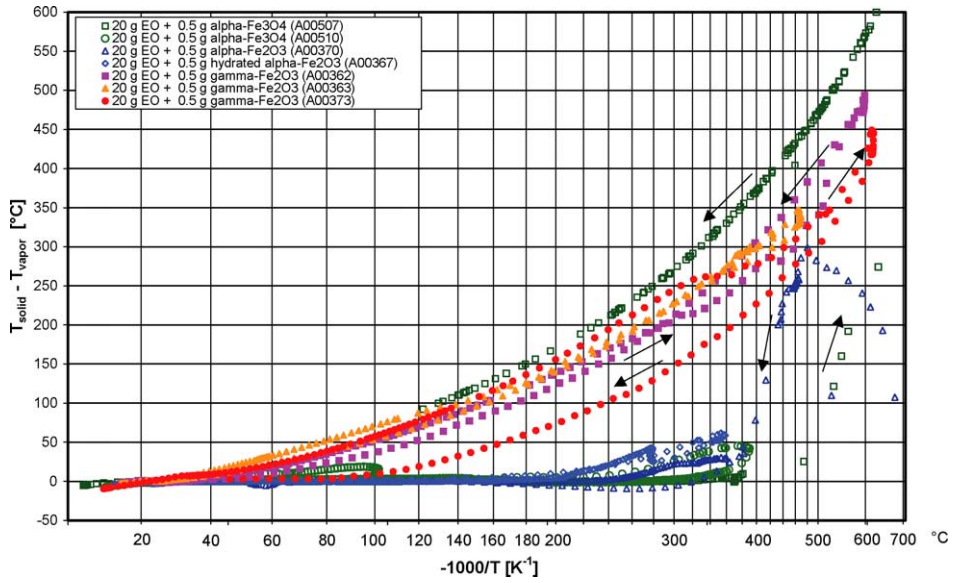
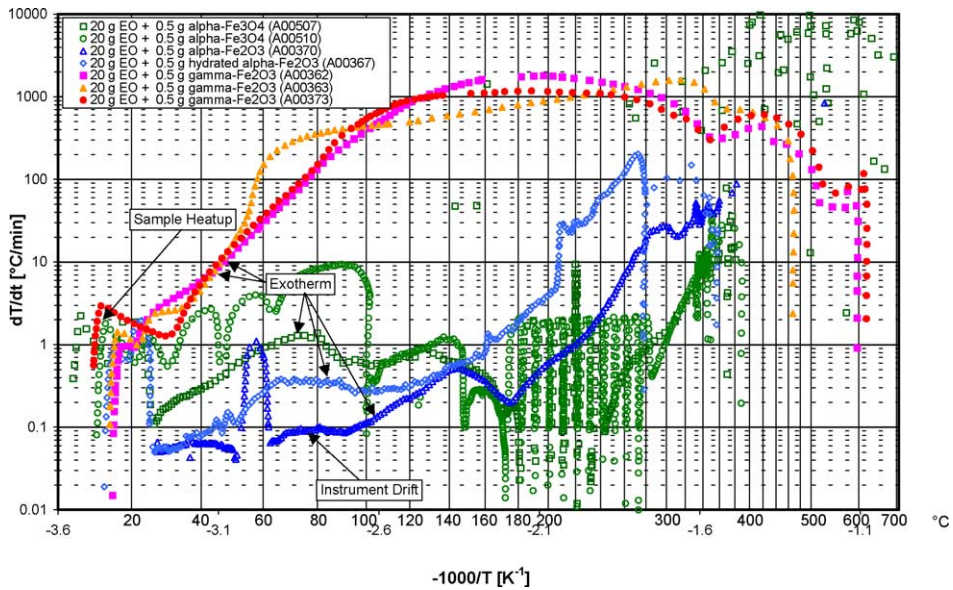Fig. 10. Temperature difference between solid and vapor phases of ethylene oxide in contact with iron oxide in the APTAC^{TM}.

Fig. 11. Self-heat rate profiles of ethylene oxide in contact with iron oxide in the APTAC^{TM}.
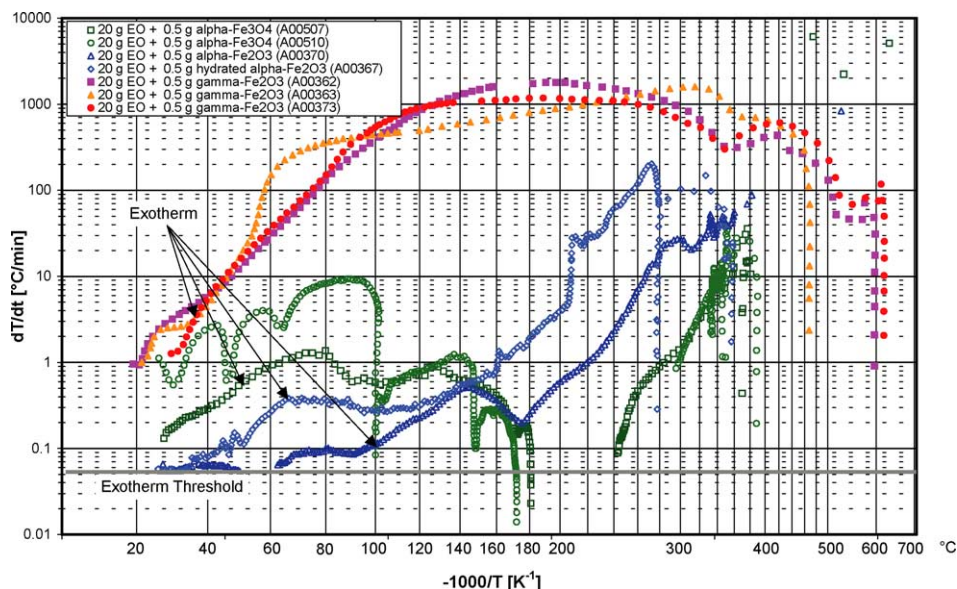
Fig. 12. Self-heat rate profiles of ethylene oxide in contact with iron oxide in the APTAC^{TM}; heat-wait-search steps removed.

From Figs. 11 and 12, it is clear that γ-Fe$_2$O$_3$ exhibits the highest reactivity of any of the samples tested. Self-heat rates of roughly 1 °C/min are seen at room temperature in the three tests of this type of iron oxide. Thereafter, acceleration to over 1000 °C/min takes place leading into a period where the rate then diminishes. It is not clear if the leveling off/decrease in the rate is actually a reaction phenomenon or just an artifact of the tests. The reaction initiates so rapidly from room temperature while the instrument is trying to stabilize the initial temperature that the heaters actually do not engage sufficiently to match the nitrogen containment vessel temperature to the sample temperature. In fact, by the time the solids temperature reaches 100–150 °C, an 80–100 °C gap has developed. At this point, the instrument effectively "gives up" and shuts off the heaters.

The next most active iron oxide material appears to be the α-Fe$_3$O$_4$ fines. A lower self-heat rate at room temperature is observed (ca. 0.1–1 °C/min), but the reaction seems to vanish shortly thereafter. Only above 240–280 °C does sustained reaction re-appear, generating rates in one case (A00507) of as high as 41,000 °C/min. In the other test (A00510), the programmed shutdown of the instrument at 360 °C seems to have arrested further reaction from taking place (which was not the case in A00507).

The hydrated α-Fe$_2$O$_3$ fines barely have a detectable exotherm at room temperature, increasing to nearly 0.4 °C/min around 70 °C. The self-heat rate remains nearly constant until about 120 °C and begins to accelerate thereafter, reaching a peak of roughly 200 °C/min. The α-Fe$_2$O$_3$ fines appear to show no exothermic activity around room temperature. Instead, a relatively unchanged self-heat rate ranging from 0.06 to 0.1 °C/min (which is likely drift) is observed. At 95 °C, an exotherm appears, giving a self-heat rate up to 0.5 °C/min, and then dropping off, until a second exotherm starts at 175 °C. The behavior of the α-Fe$_2$O$_3$
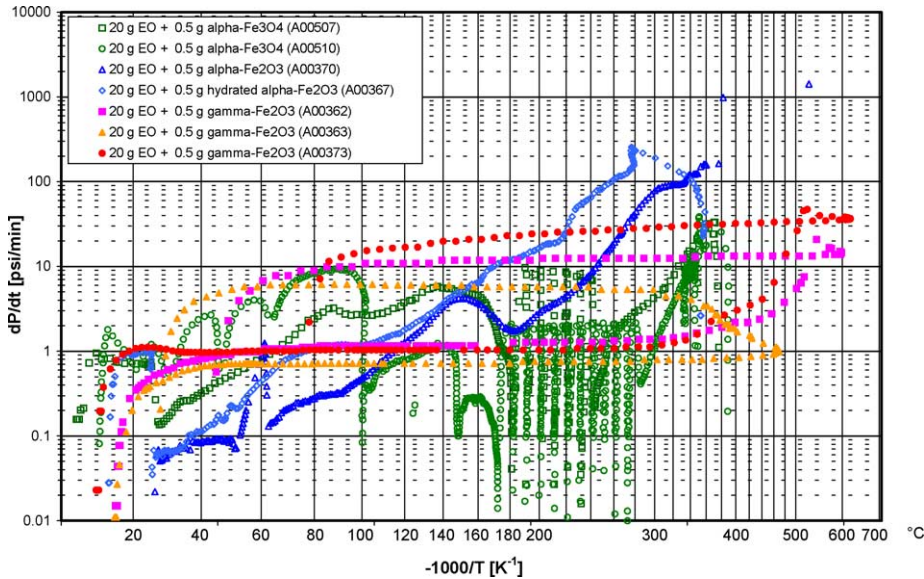
Fig. 13. Pressurization rate profiles of ethylene oxide in contact with iron oxide in the APTAC^{TM}.

fines appears to parallel that of the hydrated α-Fe$_2$O$_3$ fines except for being displaced to 50–60 °C higher temperature.

The corresponding pressurization rate versus reciprocal temperature data of Fig. 13 highlight the distinction between the solids temperature and the liquid or gas-phase temperature. For tests in which the temperature difference between the gas and solid phases is not substantial, such as the α-Fe$_3$O$_4$, hydrated α-Fe$_2$O$_3$, and α-Fe$_2$O$_3$ tests, the pressurization rate data parallel the trends displayed in the self-heat rate plots in both qualitative shape and relative order or reactivity. In these tests, the liquid temperature can be expected to be comparable to the gas temperature and therefore the solids temperature (at least, for temperatures below about 400 °C). The vapor pressure of the liquid ethylene oxide is then related to the solids temperature and the pressurization rate data can be expected to be related to the ethylene oxide vapor pressure.

The γ-Fe$_2$O$_3$ tests, however, show relatively low and constant pressurization rates with temperature (up to about 350 °C). As has been demonstrated in Fig. 10, the solids can have hundreds of degrees higher temperature than the gas and liquid phases. Therefore, the link between the solids temperature and the ethylene oxide vapor pressure exerted by the liquid is weak. Above 350 °C, ethylene oxide decomposition is expected to become prominent and provide an additional means for pressure generation in the system.

The pressure versus temperature plots in Fig. 14 also characterize pressure generation in the system. For the most part, the α-Fe$_3$O$_4$, hydrated α-Fe$_2$O$_3$, and α-Fe$_2$O$_3$ tests follow the projected curve of ethylene oxide vapor pressure + nitrogen pad gas pressure (adjusted for gas volume and temperature). At about 170 °C, the pressures from these tests fall away from the projected pressure, presumably because of ethylene oxide consumption and/or the increasing difference between solids and gas/liquid temperature. Note that during cool-down,
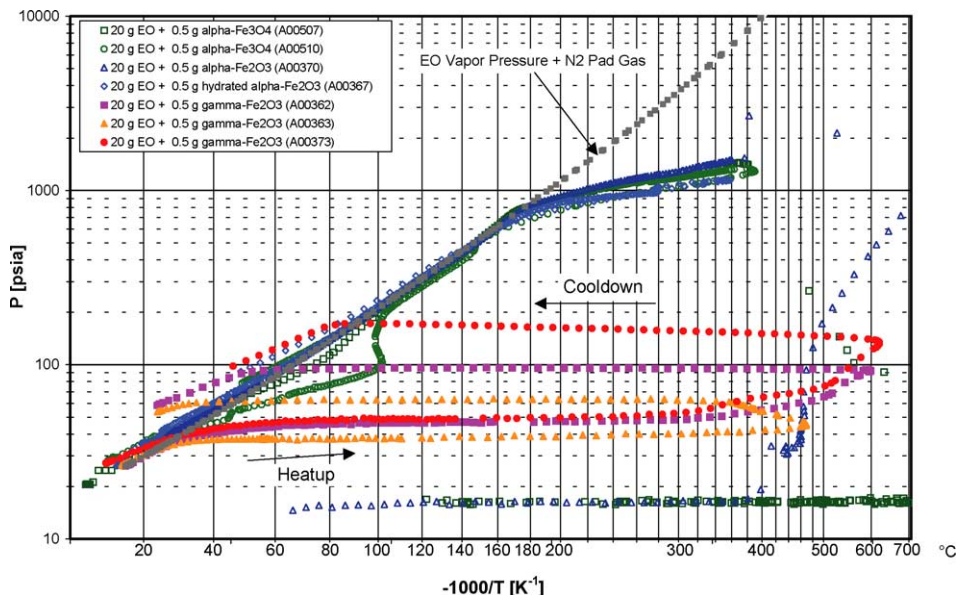
Fig. 14. Pressure–temperature profiles of ethylene oxide in contact with iron oxide in the APTAC^{TM}.

the pressures in tests A00370 and A00507 fall to and remain well-below 20 psia (138 kPa). This is due to rupture of the titanium cell with subsequent bursting of the containment vessel rupture disk causing de-pressurization to atmospheric pressure. Although these experiments were not intended to study ethylene oxide ignition, examination of the behavior of test A00370 at about 380 °C in Figs. 13 and 14, reveals sharp increases in pressurization rate and pressure, respectively, suggesting that ignition might be taking place.

In the γ-Fe$_2$O$_3$ tests, deviation from the projected vapor pressure + gas pad line begins by 30 °C and no noticeable increase in pressure occurs until the solids reach 350 °C. Even on a plot that references the gas-phase temperature (instead of the solids temperature), the same behavior is seen, though it is less pronounced. Above 350 °C, an increase in pressure is observed until the experiment is ended (through shutdown of the heaters) and the pressure stays generally constant during cool-down. Once below 80 °C, the pressure begins to fall again, possibly signaling the condensation of some vapor species. Nevertheless, the pressures observed during cool-down at a particular temperature always remain higher than the corresponding pressures during heat-up, indicating generation of non-condensable species.

The rapidity of the exotherm of ethylene oxide in the presence of γ-Fe$_2$O$_3$ is illustrated in the time-to-maximum rate plot of Fig. 15. At room temperature, it takes less than 10 min for the rate to reach its maximum; by 44–50 °C, the time is only about 1 min. The next most active form of iron oxide from this perspective is the α-Fe$_3$O$_4$. On the order of 0.5–2 h time from room temperature is required to reach 100 °C. However, because the exotherm diminishes thereafter and effectively disappears at 180 °C, secondary curves for the experiments are shown for temperatures between 240 and 300 °C. In the latter case, the time required to reach the overall maximum (around 380 °C) is longer than that for the
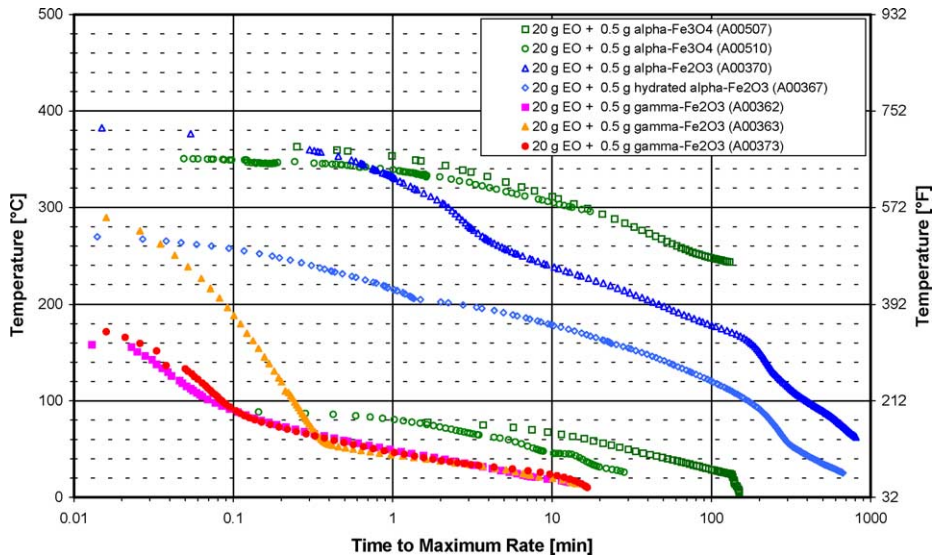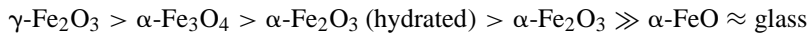
Fig. 15. Time-to-maximum rate profiles of ethylene oxide in contact with iron oxide in the APTAC^{TM}.

Fe_2O_3 and hydrated Fe_2O_3 solids. The Fe_2O_3 and hydrated Fe_2O_3 solids require several hours to reach their maximum rates when starting below 100 °C.

3.3. Implications

The results of this study clearly demonstrate the reactivity of ethylene oxide with certain iron oxides. When ethylene oxide is heated in the absence of contaminants, exothermic activity is typically not observed until about 190–250 °C [3]. The reactivity seen in this study can be attributed to the polymerization and disproportionation reactions of ethylene oxide referenced in an earlier study [6] as well as direct reaction of ethylene oxide with the iron oxide, changing the oxidation state of the iron oxide and producing methane, ethane, carbon, CO, or CO_2. Exothermic reaction when iron oxide and ethylene oxide are together, can occur at temperatures below 100 °C and even as low as room temperature. The calorimetry tests suggest the following relative reactivities of iron oxides with ethylene oxide:

$$\gamma\text{-}Fe_2O_3 > \alpha\text{-}Fe_3O_4 > \alpha\text{-}Fe_2O_3 \text{ (hydrated)} > \alpha\text{-}Fe_2O_3 \gg \alpha\text{-}FeO \approx \text{glass}$$

It is interesting that one form of iron oxide, namely FeO, was found to have no detectable reactivity with ethylene oxide in the temperature range probed and within the sensitivity of the instrument.

In unpublished results of Chippett [8], ethylene oxide combined with $\gamma\text{-}Fe_2O_3$ also leads to significant exothermic behavior (that is, over 1 °C/min) at approximately room temperature and is most reactive of the ethylene oxide–iron oxide combinations examined. The order of relative activities of the remaining iron oxides differs, though. In the previous study, the tests included steps to "soak" the solids with ethylene oxide at a particular temperature

and to provide external heating to promote propagating ethylene oxide decomposition in the test cell. It is not surprising that the order of "ease of ignition" of ethylene oxide found in that study (i.e. γ-Fe$_2$O$_3$ > α-Fe$_2$O$_3$ > hydrated α-Fe$_2$O$_3$ > Fe$_3$O$_4$) differs from the current study.

The surface area of the iron oxide is expected to be an important factor in determining the reactivity with ethylene oxide. In the work of Chippett, high surface area α-Fe$_3$O$_4$ was found to facilitate ethylene oxide ignition more readily than the low surface area counterpart. In the present study, unfortunately, surface areas have not been measured and therefore, this characteristic cannot yet be factored into the relative reactivities of the iron oxides.

The investigation of the 1991 explosion at the Seadrift, Texas ethylene oxide plant explosion focused on the role ethylene oxide polymer and the gamma form of Fe$_2$O$_3$, which exhibits the highest reactivity with ethylene oxide and does so essentially at ambient temperatures, may have had in the incident. While it is still unclear how this particular iron oxide structure is formed, it is evident that its presence poses a safety concern for ethylene oxide-containing equipment. Moreover, other common forms of iron oxides, such as α-Fe$_3$O$_4$ and α-Fe$_2$O$_3$, clearly can react with ethylene oxide at temperatures within reach of standard ethylene oxide processing conditions. Perhaps the relative infrequent occurrence of events of this type can be related to another important effect—the role of thermal inertia.

3.4. Thermal inertia effects

The uptake of reaction heat by processing equipment, as characterized by thermal inertia, acts to dampen the extent of temperature rise resulting from the reaction. Ethylene oxide reaction with iron oxide fines has occurred in purification equipment where the iron oxide is neither in contact with large quantities of ethylene oxide nor, it is believed, in thermal contact with the equipment metallurgy (due to physical separation as well as formation of an encapsulating insulating polymer layer). It is possible that, in most cases, where such iron oxides are exposed to ethylene oxide, there is sufficient equipment metal present (for example, the equipment wall or equipment internals, such as trays), combined with the small amounts of resident liquid and iron oxide, that the effective thermal inertia is much higher than that probed in these calorimetric tests. If this were the case, most reaction exotherms that might occur would be accompanied by only modest temperature and pressure rises and may not even be observed by operating personnel. However, in situations where the reaction could develop and heat absorption by surrounding equipment is reduced, the opportunity for significant equipment damage and personnel injury can be significant.

4. Summary

Testing of ethylene oxide in the presence of various iron oxide fines has revealed exothermic reactivity at temperatures as low as room temperature. Samples of FeO, α-Fe$_3$O$_4$, α-Fe$_2$O$_3$ (hydrated), α-Fe$_2$O$_3$, and γ-Fe$_2$O$_3$ were suspended in a basket above ethylene oxide liquid in a test cell for characterization via adiabatic calorimetry. The γ-Fe$_2$O$_3$, identified in previous studies as a contributing factor in the 1991 Union Carbide Seadrift incident, was found to exhibit higher reactivity with ethylene oxide than the other iron oxide fines tested.

Ethylene oxide in combination with all of the above iron oxide fines, except FeO, displays exothermic activity below 100 °C. The temperature of the fines in many cases ultimately exceeded the gas-phase temperature by 300–600 °C (α-Fe$_3$O$_4$, α-Fe$_2$O$_3$, and γ-Fe$_2$O$_3$). Self-heat rates approaching 2000 °C/min were observed for the γ-Fe$_2$O$_3$ fines while rates in excess of 100 °C/min were found for some of the other fines (α-Fe$_2$O$_3$—standard and hydrated). In two cases (α-Fe$_3$O$_4$ and α-Fe$_2$O$_3$), pressurization rates above 1000 psi/min (6890 kPa/min) took place. A sample of FeO displayed no evidence of significant reactivity with ethylene oxide. The impact of fines surface area, which is believed to substantially influence the overall reaction rate, was not probed in this study.

While calorimetric testing reveals considerable activity between ethylene oxide and certain iron oxides at rather modest temperatures, thermal inertia effects, such as heat uptake by equipment to which fines may be attached in commercial operation, are presumed to be a factor in limiting the occurrence of related exotherms in ethylene oxide manufacturing facilities.

References

[1] L.G. Britton, Thermal stability and deflagration of ethylene oxide, Plant/Operat. Prog. 9 (2) (1990) 75–86.

[2] Ethylene Oxide User's Guide, second ed., August 1999.

[3] G.A. Melhem, A. Gianetto, M.E. Levin, H.G. Fisher, S. Chippett, S.K. Singh, P.I. Chipman, Kinetics of the reactions of ethylene oxide with water and ethylene glycols, Proc. Safety Prog. December (2001).

[4] G.A. Viera, P.H. Wadia, Ethylene oxide explosion at seadrift, Texas. Part I. Background and technical findings, in: Proceedings of the 27th Annual Loss Prevention Symposium, AIChE, April 1993.

[5] L.L. Simpson, P.E. Minton, Ethylene oxide explosion at seadrift, Texas. Part II. Reboiler safety, in: Proceedings of the 27th Annual Loss Prevention Symposium, AIChE, March 1993.

[6] B.C. Ream, E.M. Thorsteinson, S. Chippett, D.J. Schreck, J.B. Cropley, G.B. Elder, Ethylene oxide explosion at seadrift, Texas. Part III. Iron oxide chemistry, in: Proceedings of the 27th Annual Loss Prevention Symposium, AIChE, March 1993.

[7] G.A. Viera, L.L. Simpson, B.C. Ream, Lessons learned from the ethylene oxide explosion at seadrift, Texas, Chem. Eng. Prog. 89 (8) (1993) 66–75.

[8] S. Chippett, Gas/Solid Reactions in the APTAC^{TM}: EO + Iron Oxides, Presentation to the DIERS (Design Institute for Emergency Relief Systems), Users Group Meeting, 1 Feburary 1995, Orlando, FL.